11th International Symposium on Turbulence and Shear Flow Phenomena (TSFP11)
Southampton, UK, July 30 to August 2, 2019

THE DIAGNOSTIC PLOT AS A MEASURE OF DEPARTURE FROM EQUILIBRIUM IN TURBULENT WING-BODY JUNCTION FLOWS

Spencer J. Zimmerman
Department of Mechanical Engineering
University of Melbourne
Parkville, Victoria 3010, Australia
zimmermans@unimelb.edu.au

Sylvia K. Romero
Department of Mechanical Engineering
University of Melbourne
Parkville, Victoria 3010, Australia
sylviar@student.unimelb.edu.au

Jimmy Philip
Department of Mechanical Engineering
University of Melbourne
Parkville, Victoria 3010, Australia
jimmyp@unimelb.edu.au

Joseph C. Klewicki
Department of Mechanical Engineering
University of Melbourne
Parkville, Victoria 3010, Australia
klewicki@unimelb.edu.au

ABSTRACT

The 'alternate' diagnostic plot introduced by Alfredsson *et al.* (*Phys. Fluids*, vol. 23, 041702, 2011) is used as a benchmark to locally evaluate the departure of turbulent wing-body junction flow wakes from 'equilibrium' boundary layers. Experimental measurements of the streamwise and transverse velocity components have been acquired in three spanwise/wall-normal planes in the wakes of both a streamlined 'wing' and a bluff 'wing' junction. Both obstacles produce a secondary flow of Prandtl's first kind, which disrupts the equilibrium implied by the universality of the alternate diagnostic plot. The obstacle wake itself (away from the junction) also disrupts this equilibrium. It is found that with downstream development the flow eventually recovers to the base zero-pressure-gradient boundary layer 'equilibrium', and that this recovery process emanates from the near-wall region.

INTRODUCTION

The 'alternate' diagnostic plot (hereafter referred to as the AD plot) introduced by Alfredsson *et al.* (2011) shows the local turbulence intensity (i.e. the root mean square of the streamwise velocity u_{rms} divided by the local mean streamwise velocity U) as a function of the local mean velocity U scaled by the free-stream velocity U_o. The original version of this representation was proposed by Alfredsson & Örlü (2010) as a means to identify potentially flawed experimental zero-pressure-gradient (ZPG) turbulent boundary layer data. This use also applies to the AD plot, since it stems from the fact that neither the explanatory nor the response variables depend on wall-distance, the boundary layer thickness, or the wall-shear-stress-based scales. Removal of dependence on these scales allows for direct inspection of the quality of the velocity measurements themselves, since all are subject to their own measurement errors independent of those of the measured velocity. The wall distance (and the need for a length scale along with it) is removed from consideration by taking advantage of the fact that U increases monotonically with wall-distance, and performing a coordinate stretching/transform such that $u_{rms}(y)$ becomes $u_{rms}(U(y))$, or simply $u_{rms}(U)$. Alfredsson *et al.* (2011) found that ZPG boundary layer profiles spanning nearly two decades in Reynolds numbers all feature a 'sub-domain' (on the alternate diagnostic plot) where the data are closely approximated by a single universal curve. The upper bound of this sub-domain is the upper limit of the total domain (i.e. $U/U_o = 1$), while the lower bound decreases as Reynolds number increases (from $U/U_o \approx 0.75$ at $Re_\theta \approx 1000$ to $U/U_o \approx 0.5$ at $Re_\theta \approx 80000$, cf. figure 4 for an example at $Re_\theta \approx 6500$). The single-curve behaviour over this domain is indicative of quasi-self-preserving development in the boundary layer over a physical domain that is stretched by the coordinate transform noted above (whereby $U(y)$ replaces y). Townsend (1976) writes that self-preserving development "embodies the principal of moving equilibrium". In this conception, the eddies at a given downstream position are the result of similar eddies from further upstream that have developed in space and intensity to degrees that are reflected in the locally relevant length and velocity scales. The 'equilibrium' revealed by the AD plot can therefore be understood to reflect an underlying structure of self-similar development in canonical turbulent boundary layers. As such, one expects that a change in the mechanisms of eddy generation manifests as a departure from the particular 'equilibrium' associated with ZPG boundary layers. That is, one would not expect a turbulent jet flow to obey the same equilibrium as is implied by the AD plot for the boundary layer. It is for this reason that we employ the AD plot from Alfredsson *et al.* (2011) as, in the words of Alfredsson & Örlü (2010), a "litmus test" to identify local departures from the boundary layer 'equilibrium'.

In this study, the AD plot is used as a benchmark to characterise departures in turbulent wing-body junction flows from the base ZPG 'equilibrium'. Junction flows are generated by the impingement of a turbulent boundary layer upon a wall-mounted obstacle. These flows are of interest not only due to their direct practical significance (e.g. submarine sails, submerged bridge piers, aircraft wing roots), but also because they present an opportunity to probe

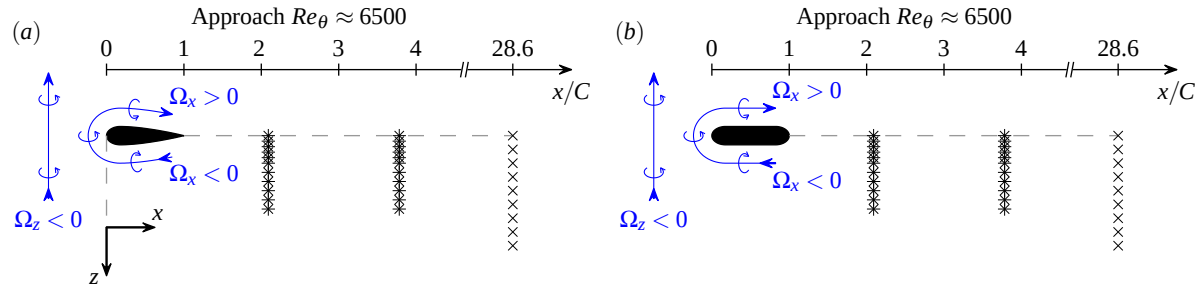

Figure 1. Plan view (wall-parallel) diagram of the present experiments and measurement locations. Positions marked by the '$\times$' and '$+$' symbols represent locations where a 'profile scan' of at least 10 wall-normal positions was collected with the 3-wire probe in the (u,v) and (u,w) orientations, respectively. The blue text and arrows illustrate the skewing of the approach boundary layer mean vorticity (i.e. $\Omega_z < 0$) into the streamwise direction, resulting in a secondary flow of Prandlt's first kind (note, however, that these sketches do not represent the actual direction of the mean vorticity vector).

the complex response of a turbulent flow field to a three-dimensional perturbation in general. The perturbations associated with the present geometries include both an embedded streamwise 'vortex' secondary flow (of Prandlt's first kind, from skewing the incident boundary layer vorticity, cf. the blue curves in figure 1) as well as a momentum deficit associated with the wake of the obstacle itself.

Downstream of the obstacle, the secondary flow can be characterised as a pair of embedded 'co-flow down' streamwise vortices that redistribute momentum, Reynolds stress, and all other quantities for which the wall-normal gradient $\partial/\partial y$ is non-zero. This redistribution is associated with the wall-normal mean advective term $V\partial(\cdot)/\partial y$ present in all transport equations. The cross-sectional area of these vortices increases downstream roughly in proportion to the (squared) boundary layer height since both depend on turbulence diffusion, e.g. see Shabaka *et al.* (1985), Fleming *et al.* (1991). The overall circulation, however, decreases only very slowly, as it is reduced only by the spanwise component of the wall shear stress, e.g. see Shabaka *et al.* (1985), Pauley & Eaton (1988). Although the broad picture of the development of boundary-layer-embedded co-flow-down vortices has been established, it is less clear how the turbulent flow field locally adjusts to changes in the mean flow field, or the degree to which changes in both are 'synchronised'. In addition to identifying departures from the boundary layer 'equilibrium', as discussed above, the diagnostic plot can be used to identify 'asynchronous' changes in the mean and fluctuating velocity fields, since replacing wall-distance with an 'intrinsic' coordinate system based on local mean velocity compensates for the effects of their mutual advection. Locations within the junction flow wakes which do not follow the boundary layer 'equilibrium' implied by the AD plot are therefore interpreted as a departure from ZPG boundary layer self-similarity, but also as having been subjected to effects beyond simple mean advection. The latter interpretation is based on the fact that simply changing the location where a set of u_{rms} and U values are observed does not change their representation on the AD plot.

EXPERIMENTS

All of the present data, summarised in figure 1, were collected in the Flow Physics Facility (FPF) at the University of New Hampshire. The FPF features a 72m fetch, making it the largest zero-pressure-gradient boundary layer wind tunnel in existence (Vincenti *et al.*, 2013). The scale of the FPF allows for development of high Reynolds numbers boundary layers without generating scales too small to be resolved by conventional measurement techniques.

Two obstacles were tested to permit an investigation into the role of the obstacle wake on the overall wing-body junction wake. Both obstacles featured a 3:2 semi-elliptic 'nose' with a maximum thickness of $T = 0.25$m and chord length $C = 1.05$m. Beyond the point of maximum thickness, however, one obstacle tapers to a point following the NACA 0020 profile while the other remains at a constant thickness before terminating in another 3:2 semi-ellipse. The flow around the streamlined obstacle, also known as a 'Rood wing', remains attached, while that around the other obstacle is expected to separate. In both cases, the approaching boundary layer featured a Reynolds number based on momentum deficit thickness θ and free-stream velocity U_o of $Re_\theta \approx 6500$. For the cases presented herein with $U_o \approx 7$ m/s, the ratio of approaching boundary layer θ to obstacle thickness T is ≈ 0.06. Data were collected in three spanwise/wall-normal planes located 2.1, 3.8, and 28.6 chord lengths downstream of the leading edge of each obstacle. Unperturbed, the boundary layer would normally develop over this range from $Re_\theta \approx 8100$–19300.

Data were collected with a custom 3-sensor hot-wire probe based on a design originally described by Kawall *et al.* (1983). This probe is composed of a standard orthogonal $\times$-wire array with one un-slanted normal wire between the two slanted wires. As with a standard $\times$-wire design, this probe is capable of resolving the streamwise component of velocity along with one transverse component—the additional wire mitigates errors associated with large instantaneous flow angles. The probe may be operated to simultaneously measure u and v, or rotated 90° about the streamwise axis to simultaneously measure u and w. The '$\times$' symbols in figure 1 demarcate locations where the probe was deployed in the (u,v) orientation, while the '$+$' symbols demarcate where data were collected using the (u,w) orientation. Wall-normal profile scans consisting of at least 10 logarithmically spaced points were collected at each '$\times$' and '$+$' symbol shown in figure 1. For comparison, multi-sensor hot-wire measurements of the unperturbed ZPG boundary layer are also available at each of the streamwise measurement stations.

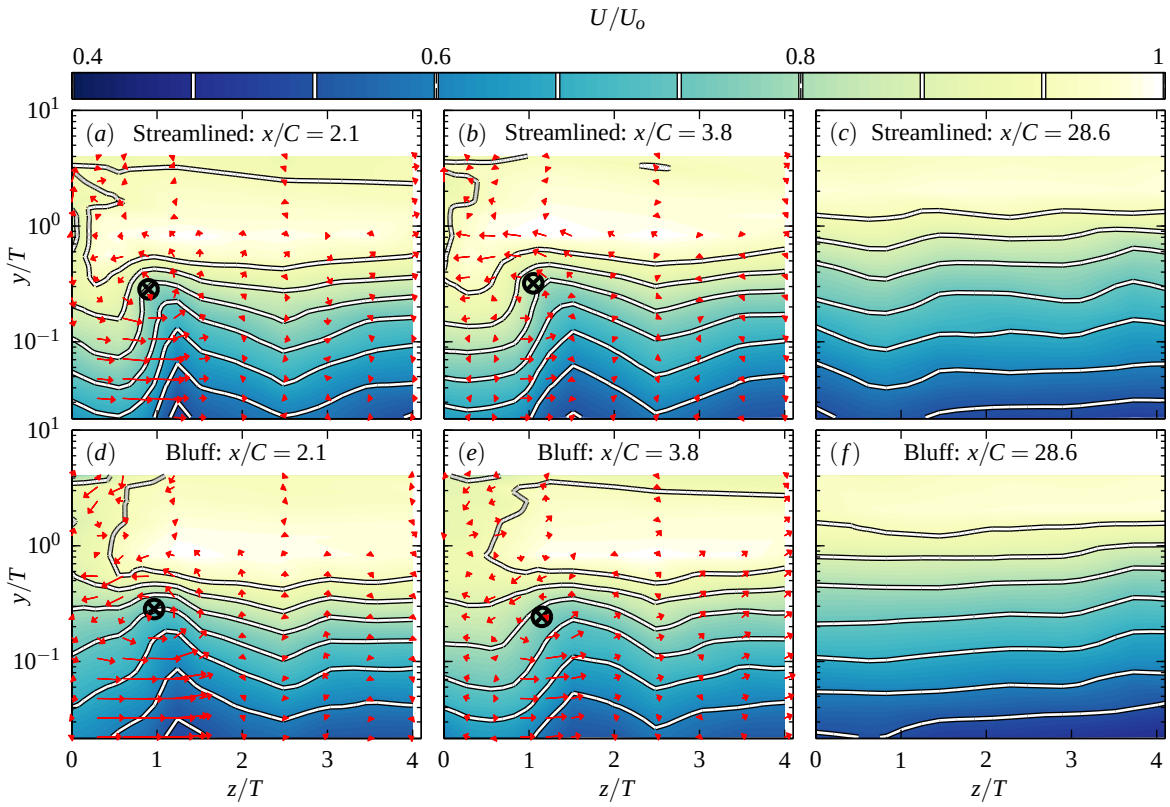

Figure 2. Contours of mean streamwise velocity normalised by the free-stream velocity U_o, along with (where available) vectors representing the mean wall-normal and spanwise velocities V and W, respectively. The vector scaling is constant throughout all regions of all sub-plots, and the longest vectors shown correspond to $(V^2+W^2)^{1/2} \approx 0.08U_o$.

RESULTS

In this section, we first discuss features of the mean velocity and mean streamwise velocity variance for the three streamlined obstacle and three bluff obstacle measurement planes. These features are then used to provide context to a discussion of the features exhibited by the data when shown in AD plot form.

Contours of the mean streamwise velocity of all three planes downstream of the streamlined and bluff obstacles are shown in figures 2(a)–(f). The two near-wake planes for both obstacles also include vector fields corresponding to the mean wall-normal and spanwise velocities, V and W respectively. The vector field scaling is constant in space (despite the log-scaling on the ordinate) and across sub-plots, with the longest vectors shown corresponding to a velocity magnitude about 8% of U_o. The vector origins also indicate the locations of each hot-wire measurement. Figures 2(a), (b), (d), and (e) clearly show the relationship between the secondary flow streamwise 'vortex' and the lifting/thinning of the streamwise velocity contours from the associated upwash/downwash flow. Also shown via the encircled $\times$ symbols on the same plots are the qualitative centrepoints of the secondary flow vortex based on the vector field. These symbols will be replicated in the subsequent figures to show the proximity of various features to the mean vortex position. Qualitatively, there is very little difference between the top and bottom rows of figure 2, which respectively represent the flow downstream of the streamlined and bluff obstacles. That said, the bluff body wake does appear to be associated with a wider momentum deficit in the region bounded by $0.5 \leq y/T$ and $0 \leq z/T \leq 1$. Although less pronounced than the near-wake planes, spanwise heterogeneity is still visible in the U contours shown in figures 2 (c) and (f) which represent the flow field at $x/C = 28.6$.

Figure 3 shows the streamwise velocity variance normalised by $U_{\tau,Z}$, the friction velocity associated with the unperturbed ZPG boundary layer at the same streamwise position. The friction velocity is used here so that the values can be compared more directly to existing ZPG velocity variance results. In contrast to the mean streamwise velocity contours shown in figure 2, the contours of $\overline{u^2}$ for the two near-wake streamlined obstacle cases exhibit clear differences with those of the bluff obstacle cases at the same locations. The downwash associated with the secondary flow downstream of the streamlined obstacle promotes entrainment of flow with very low variance (characteristic of the wake region of the ZPG boundary layer), whereas no such 'reservoir' of low-variance flow exists near $z/T = 0$ in the bluff obstacle cases owing to the separated wake of the obstacle itself. Thus, there is no clear region of 'ingested' low-variance flow in the bluff obstacle wake as there is in the streamlined obstacle wake. This suggests that the secondary flow vortex may lose coherence more rapidly downstream of the bluff obstacle than downstream of the streamlined obstacle. Far downstream, the flow directly behind both obstacles appears to have slightly elevated variance relative to the flow further outboard, indicating (as with the mean streamwise velocity) that the flow has not completely returned to a spanwise-homogeneous state.

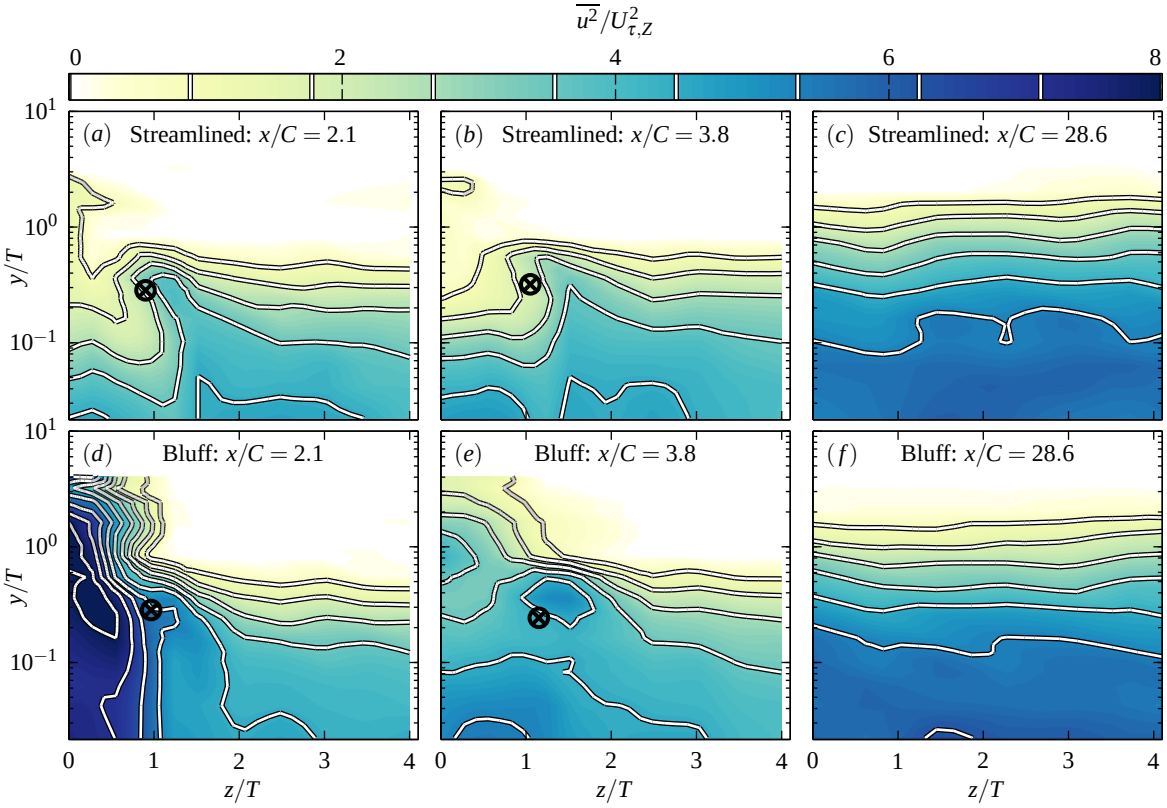

Figure 3. Streamwise velocity variance normalised by the approaching boundary layer friction velocity $U_{\tau,A}$, as measured at the location of the leading edge of the obstacle without the obstacle present. All values are therefore normalised by the same constant, and not by a U_τ that decreases with increasing downstream distance.

A selection of the present data is shown in alternate diagnostic (AD) plot form in figure 4. Also shown in figure 4 is the $Re_\theta \approx 6500$ boundary layer DNS data of Sillero *et al.* (2013) for comparision to the present ZPG benchmark measurements. The quasi-self-preserving sub-domain for the DNS Reynolds number begins at $U/U_o \approx 0.6$, where the data appear to merge with the dashed line in figure 4, given by Alfredsson *et al.* (2011) as:

$$\frac{u_{rms}}{U} = 0.031 + 0.260\left(1 - \frac{U}{U_o}\right). \qquad (1)$$

As expected, the present unperturbed boundary layer measurements at $Re_\theta \approx 8100$ fall almost directly on top of the DNS data over the quasi-self-preserving range. Large deviations from the unperturbed curve are seen in the bluff obstacle data that, as will be shown in figure 5, correspond to the region directly behind the obstacle. Although the deviations of the streamlined obstacle data from the ZPG boundary layer equilibrium curve appear small, given the agreement between the experimental and DNS unperturbed cases, these deviations can be considered significant.

Figure 5 shows the difference (as a function of space) between each measured velocity signal when represented in AD plot form and the expected value for the unperturbed boundary layer at the same U/U_o. In other words, figure 5 shows the spatial dependence of the difference between the coloured dots and the lines that connect the white squares at the same U/U_o for each of the six cases plotted in figures 2 and 3. For the two planes in the near-wake of the streamlined obstacle, the flow directly below the vortex 'centre' falls below the 'self-similar' curve on the AD plot, while the opposite is true for the flow directly above the vortex 'centre'. The largest deviations from the unperturbed self-similar curve in the vicinity of the vortex 'centre' therefore do not occur in either the 'upwash' or 'downwash' re-

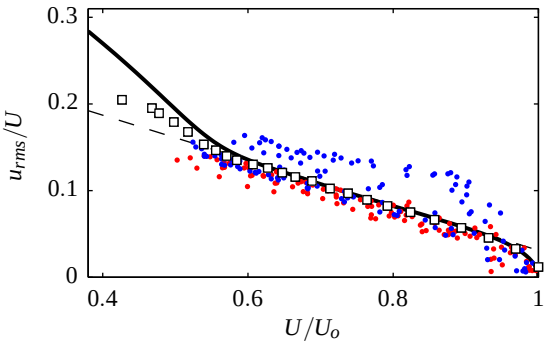

Figure 4. Alternate diagnostic (AD) plot (Alfredsson *et al.*, 2011) for: —— : boundary layer DNS of Sillero *et al.* (2013) at $Re_\theta \approx 6500$; '□': present ZPG boundary layer measurements at $Re_\theta \approx 8100$; • : present streamlined obstacle measurements at $x/C = 2.1$; • : bluff obstacle measurements for $x/C = 2.1$. The dashed black line corresponds to equation 1 as given by Alfredsson *et al.* (2011).

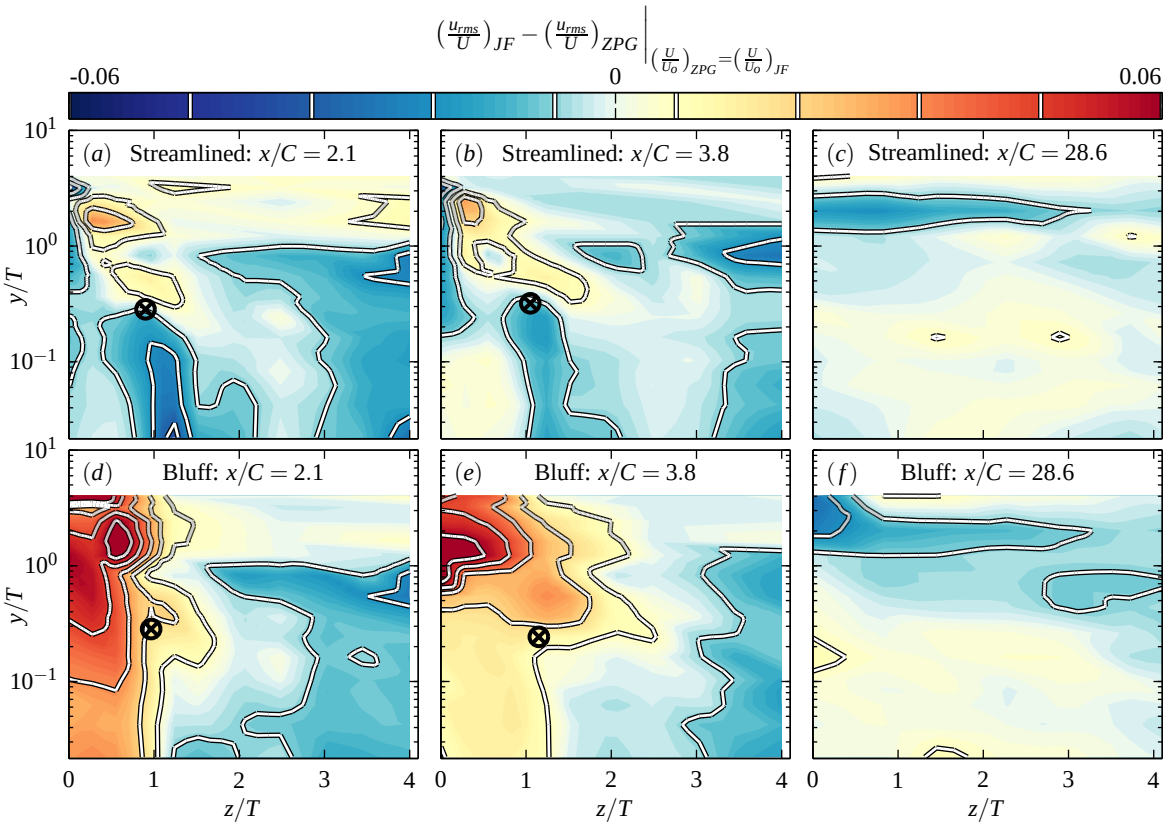

Figure 5. Spatial dependence of difference in turbulence intensity between junction flow (subscript JF) and ZPG boundary layer (subscript ZPG) at matched mean velocity U/U_o. Sub-figures $(a)/(d)$, for example, respectively represent the spatial dependence of the difference (as shown in figure 4) between the red/blue dots and the curve that passes through the white squares.

gions, but rather in the intersecting flow between the two, where the secondary flow is mostly horizontal (i.e. in the $\pm z$-direction). This is consistent with the notion that the boundary layer 'equilibrium' is maintained (at least somewhat) throughout the initial advective transport, but that it is eventually destroyed where flow originating from above meets flow originating from below.

The near-wake planes downstream of the bluff obstacle show clear deviation from the boundary layer equilibrium within the wake of the obstacle itself. The region immediately behind the obstacle deviates from the boundary layer equilibrium because the local momentum deficit and level of turbulence intensity are reflective of the dynamics of the separated wake flow rather those of the boundary layer. As the wake of the obstacle widens with downstream distance, so too does the region where the AD plot points exceed the boundary layer equilibrium curve.

Although less distinct than in the streamlined obstacle cases, there does appear to be a region of positive deviation from the boundary layer AD curve above the vortex centre for the two near-wake bluff obstacle cases. The negative deviation region observed below the vortex centre in the streamlined obstacle cases, however, is not replicated in the bluff obstacle cases. This is reflective of the lack of low-variance flow near $z/T = 0$ to be 'ingested' by the secondary flow as noted above, and the consequent higher $\overline{u^2}$ in the 'downwash' region of the secondary flow compared to the streamlined obstacle case.

The magnitude of the deviations from the boundary layer AD plot curve decrease near the wall moving downstream from $x/C = 2.1$ to $x/C = 3.8$ for both obstacles. This suggests that the equilibrium in that domain is at least partly maintained/enforced by the conditions at the wall. Given the knowledge that the boundary layer equilibrium is not entirely maintained by the outer flow conditions, it stands to reason that the relaxation appears to occur more rapidly near the wall, since the turbulence time scales in that region are shorter than those further from the wall.

Essentially all of the flow within the boundary layer (i.e. that having any appreciable $\overline{u^2}$) returns to the equilibrium curve by the time it has traveled to the $x/C = 28.6$ measurement station. The darker blue regions in figures $5(c)$ and (f) between $0 \leq z/T \leq 3$ correspond to a region of slightly reduced velocity relative to U_o (which is taken here as the maximum measured velocity) but essentially zero variance. This is likely the remnant of the two-dimensional obstacle wake, where the mean deficit remains, while the turbulence has decayed.

CONCLUSIONS

The alternate diagnostic plot introduced by Alfredsson *et al.* (2011) contains a sub-domain upon which velocity data from zero-pressure-gradient boundary layers spanning nearly two decades in Reynolds number satisfy a similarity solution. The existence of this similarity solution implies that the development of ZPG boundary layers (on the applicable sub-domain) is quasi-self-preserving, or equiv-

alently that it obeys a "moving equilibrium" (Townsend, 1976). Since this 'equilibrium' reflects the mechanisms of eddy generation associated with ZPG boundary layers in particular, local departures from the similarity solution are interpreted as reflective of mechanisms associated instead with *perturbations* to the boundary layer. On this basis, we characterise the relaxation of two wing-body junction flow wakes (back to the ZPG base case) through the lens of local departures from the boundary layer similarity solution. It is found that the largest departures from the boundary layer similarity solution are associated with the separated wake of the bluff obstacle, where local turbulence intensity levels are considerably higher at fixed U/U_o than in the ZPG boundary layer. The regions directly above and below the streamlined obstacle secondary flow 'vortex centre' clearly deviate from the boundary layer similarity solution at $x/C = 2.1$ and $x/C = 3.8$, while those adjacent to the centre do not. This suggests that the 'equilibrium' is maintained through the initial 'mutual advection' of u_{rms} and U, but that it is disrupted at the interfaces between flow originating from above and flow originating from below. Deviations from the boundary layer similarity solution near the wall relax more rapidly from the $x/C = 2.1$ plane to the $x/C = 3.8$ plane than those further from the wall. This suggests that the associated 'equilibrium' is maintained (at least in part) by the conditions at the wall.

ACKNOWLEDGEMENTS

This work was supported by the Australian Research Council and the Office of Naval Research under award number N00014-17-1-2307.

REFERENCES

Alfredsson, P. H. & Örlü, R. 2010 The diagnostic plot—a litmus test for wall bounded turbulence data. *Eur. J. Mech. B/Fluids* **29** (6), 403–406.

Alfredsson, P. H., Segalini, A. & Örlü, R. 2011 A new scaling for the streamwise turbulence intensity in wall-bounded turbulent flows and what it tells us about the "outer" peak. *Phys. Fluids* **23** (4), 041702.

Fleming, J. L., Simpson, R. L. & Devenport, W. J. 1991 An experimental study of a turbulent wing-body junction and wake flow. VPI&SU Rep. VPI-AOE-179. Va. Polyteck. Inst. State Univ., Blacksburg, VA.

Kawall, J. G., Shokr, M. & Keffer, J. F. 1983 A digital technique for the simultaneous measurement of streamwise and lateral velocities in turbulent flows. *J. Fluid Mech.* **133**, 83–112.

Pauley, W. R. & Eaton, J. K. 1988 Experimental study of the development of longitudinal vortex pairs embedded in a turbulent boundary layer. *AIAA J.* **26** (7), 816–823.

Shabaka, I. M. M. A., Mehta, R. D. & Bradshaw, P. 1985 Longitudinal vortices imbedded in turbulent boundary layers. Part 1. Single vortex. *J. Fluid Mech.* **155**, 37–57.

Sillero, J. A., Jiménez, J. & Moser, R. D. 2013 One-point statistics for turbulent wall-bounded flows at Reynolds numbers up to $\delta^+ \approx 2000$. *Phys. Fluids* **25** (10), 105102.

Townsend, A. A. 1976 *The structure of turbulent shear flow*. Cambridge University Press.

Vincenti, P., Klewicki, J., Morrill-Winter, C., White, C. M. & Wosnik, M. 2013 Streamwise velocity statistics in turbulent boundary layers that spatially develop to high Reynolds number. *Exp. Fluids* **54** (12), 1629.